

# Time-dependent independent-particle model calculation of multiple capture and ionization processes in $p$ -Ar, $\bar{p}$ -Ar, and $\text{He}^{2+}$ -Ar collisions

T. Kirchner\*

*Max-Planck-Institut für Kernphysik, Saupfercheckweg 1, D-69117 Heidelberg, Germany*

M. Horbatsch†

*Department of Physics and Astronomy, York University, Toronto, Ontario, Canada M3J 1P3*

H. J. Lüdde‡

*Institut für Theoretische Physik, Universität Frankfurt, Robert-Mayer-Straße 8, D-60054 Frankfurt/Main, Germany*

(Received 6 August 2002; published 22 November 2002)

Previous work on multielectron transitions in proton, antiproton, and  $\text{He}^{2+}$ -ion impact on neon is extended to the case of argon targets for collision energies in the 5–1000 keV/amu range. Global quantities such as net electron loss from the target, net capture, and net ionization are predicted within experimental errors using a spherically symmetric optimized effective target atom potential with dynamical screening effects based on the time-dependent net ionization probability. The inclusion of target response is crucial in order to obtain correct positions and heights for the peaks in the net ionization cross sections. Effects due to cascading following multiple outer-shell excitation are found to be appreciable at energies between 10 and 100 keV/amu, but are overestimated by the statistical model.  $L$ -shell vacancy production is reported to affect recoil charge state production at energies above 200 keV/amu for charge states  $q \geq 3$ . At low and intermediate energies, the independent-particle model is shown to overestimate  $q$ -fold recoil ion production significantly for  $q \geq 3$  for proton impact signaling the role of electronic correlations for these channels. For antiproton impact the  $q = 3$  cross section is consistent with the independent-particle model.

DOI: 10.1103/PhysRevA.66.052719

PACS number(s): 34.50.Fa, 34.70.+e

## I. INTRODUCTION

In a previous series of papers, multiple-electron processes in medium-energy collisions with oxygen and neon targets have been investigated in a quantum-mechanical framework. A time-dependent independent-particle model (IPM) was constructed based on the stationary optimized potential method of density-functional theory. It was shown that the correct treatment of exchange effects in this model is crucial for the prediction of accurate ionization cross sections [1–3]. The calculations for multiple-electron ionization and capture from neon targets by singly charged projectiles (protons and antiprotons) were carried out with frozen target potentials. The single-particle time-dependent Schrödinger equations (TDSE) from the semiclassical approximation to the collision problem were solved by the so-called basis generator method (BGM). In this approach, the Hilbert space is divided into a  $P$  space represented by explicit target eigenstates for all occupied and some unoccupied bound states, and a  $Q$  space that is spanned by basis states generated by the repeated action of the perturbing potential onto the  $P$ -space states [4,5].

The IPM-BGM approach was applied successfully to calculate not only ionization and capture cross sections, but also single and multiple excitation of target electrons in atomic

oxygen [6]. For projectile ions with several charges, a time-dependent screening model was introduced in which the effective atomic potential maintains its spherical shape, but is made more attractive during the collision via a parametric dependence on the time-dependent ionization probability. This model was tested successfully for  $\text{He}^{2+}$ -Ne collisions [7], and it was found that the dynamical screening effects become noticeable in the net ionization cross section at energies below 200 keV/amu. Without this time-dependent screening mechanism, the experimental net electron-loss cross section is overestimated by as much as 25% at an energy of 20 keV/amu. Numerous charge-state correlated cross sections were calculated and compared with the available experimental data [8–10]. Quantitative agreement could be achieved for multiple-electron loss with multiplicities up to  $q = 3$ , while factor-of-2 discrepancies were observed in some of the charge-state correlated cross sections at this level. For higher electron multiplicities ( $q \geq 4$ ), the IPM results overestimate the experimental data substantially, which indicates that electron correlation effects become significant in this regime.

For  $\text{C}^{4+}$ -Ne collisions, this work was extended in Ref. [11] to include dynamical screening effects at the projectile as well. It was found that the net recoil ion cross section exhibits a scaling behavior when the screening effects are included and that multiple-electron loss from the target can be described by the IPM for multiplicities up to  $q = 5$ . Some serious discrepancies remained with experiments concerning the break up of the electron loss into multiple-capture and multiple-ionization contributions. This work supports the

\*Electronic address: tom@mpi-hd.mpg.de

†Electronic address: marko@yorku.ca

‡Electronic address: luedde@th.physik.uni-frankfurt.de

idea that the applicability of the IPM framework to multiple ionization of a given target atom does depend on the strength of the projectile charge.

Subsequently, the theoretical work was extended to include systems where an additional projectile electron is carried into the collision and tested on the  $\text{He}^+$ -Ne system [12]. The problem was broken up into separate projectile- and target-electron calculations with appropriate single-particle calculations for the orbitals. Remarkable results were obtained for projectile neutralization (spin effects in capture to the He singlet state) and for electron loss from the projectile (in which nontransfer from the target plays a major role). These data explained some of the experimental results [13–15] and provided evidence for the importance of Pauli blocking in an energy range of 10–200 keV/amu.

The success of the IPM-BGM calculations to describe multielectron transition cross sections in these collisions involving simple closed-shell (neon) and open-shell (oxygen) targets has motivated us to look further for more complicated target atoms for which a large amount of experimental data is also available (see, e.g., Refs. [8–10,13–16]). The extension from Ne to Ar targets involves additional complications beyond the inclusion of an  $M$  shell (in addition to the  $K$  and  $L$  shells tested in neon). Argon atoms are more polarizable than neon, and multiple excitations in the  $M$  shell (with subsequent autoionizing transitions) are much more likely to occur than in the  $L$  shell of neon. For this reason we investigated the global cross sections in collisions between argon atoms and protons, antiprotons, and helium nuclei, and report them in the present paper. For many channels these calculations provide a satisfactory theoretical explanation.

The theoretical framework will not be discussed in detail; we refer the reader to Refs. [2,7] for the details of the IPM, and to Refs. [4,5] for the BGM. Some implementation details for the BGM (as it applies to the present case) are given in Sec. II, while the computational results are discussed and compared with experiment and a few other calculations in Sec. III. Conclusions are drawn in Sec. IV with respect to the appropriateness of the IPM *vis á vis* the importance of electronic correlations in these collisions. Atomic units with  $\hbar = e = m_e = 1$  are used throughout this work.

## II. THEORY

Two main ingredients define the IPM. The first one is the replacement of the many-electron TDSE that describes the collision system in the semiclassical approximation by a set of single-particle equations,

$$i\partial_t\psi_i(\mathbf{r},t) = \hat{h}(t)\psi_i(\mathbf{r},t), \quad i=1, \dots, N. \quad (1)$$

The second one is concerned with the extraction of the relevant information from the solution of Eq. (1) and is discussed further below.

The Hamiltonian  $\hat{h}$  of Eq. (1) contains the kinetic energy, the Coulomb potentials of the target and projectile nuclei, and an effective potential  $v_{ee}(t)$  due to the electron-electron interaction. The choice of  $v_{ee}$  is decisive for the quality of the IPM; according to time-dependent density-functional

theory (TDDFT), in principle, it is even possible to choose  $v_{ee}$  such that the *exact* one-particle density  $n(\mathbf{r},t)$  of the interacting many-electron system is reproduced [17]. However, only the existence of an effective potential with this property can be proven, and thus appropriate modeling of  $v_{ee}$  is necessary in any practical calculation.

In the present study we compare two models for  $v_{ee}$ , which are described in detail in Ref. [7]: (1) the *no-response* approximation, in which  $v_{ee}$  is approximated by a stationary atomic ground-state potential obtained from the optimized potential method (OPM) [18–20], (2) the *target-response* model, in which additionally the unscreening of the target nucleus due to electron removal during the collision is taken into account in a global fashion.

In both cases the single-particle equations (1) are solved by the BGM, i.e., the orbitals  $|\psi_i(t)\rangle$  are expanded in terms of dynamically adapted basis states

$$|\psi_i(t)\rangle = \sum_{\mu=0}^M \sum_{\nu=1}^V c_{\mu\nu}^i(t) |\chi_\nu^\mu(t)\rangle, \quad (2)$$

$$|\chi_\nu^\mu(t)\rangle = [W_p(t)]^\mu |\varphi_\nu^0\rangle, \quad \mu=0, \dots, M. \quad (3)$$

Here  $W_p$  denotes the suitably regularized projectile potential. For all projectiles studied in this work, the basis includes the undisturbed target eigenstates  $|\varphi_\nu^0\rangle$  of the  $KLMN$  shells, and 93 functions from the set  $\{|\chi_\nu^\mu(t)\rangle, \mu \geq 1\}$  up to order  $\mu = 8$ , which have been orthogonalized to the set  $\{|\varphi_\nu^0\rangle\}$ . Furthermore, we have performed some test calculations with an expanded basis, which also included the bound states of the  $\text{Ar}(O)$  shell, but we found only minor variations in the results. The population of the states  $\{|\chi_\nu^\mu(t)\rangle, \mu \geq 1\}$  at the time  $t = t_f$  after the collision when summed over all initial states is interpreted as the net electron loss from the target,

$$P_{\text{net}}^{\text{loss}} = \sum_{i=1}^N p_i^{\text{loss}} = \sum_{i=1}^N \sum_{\mu=1}^M \sum_{\nu=1}^V |\langle \chi_\nu^\mu(t_f) | \psi_i(t_f) \rangle|^2. \quad (4)$$

The net capture contribution  $P_{\text{net}}^{\text{cap}}$  is extracted by projecting the propagated orbitals onto all traveling projectile states of the  $KLM$  shells, and the net ionization  $P_{\text{net}}^{\text{ion}}$  is calculated via the relation

$$P_{\text{net}}^{\text{ion}} = P_{\text{net}}^{\text{loss}} - P_{\text{net}}^{\text{cap}}. \quad (5)$$

The corresponding total cross sections are obtained after integration of the probabilities over impact parameter.

Instead of using a channel representation, one can define the net probabilities by integrals of the one-particle density  $n(\mathbf{r},t)$  over appropriate finite regions around the target and the projectile, i.e., by functionals of  $n$  [2]. From the perspective of TDDFT, this is an obvious example for a general property. According to the basic theorems *all* information (including correlated channels) should be available from  $n$  [21]. The problem is that no prescriptions are readily available for the extraction of more detailed data, such as  $q$ -fold electron loss from the target.

A straightforward approach to obtain such information is based on a physical interpretation of the single-electron orbitals. This is the second ingredient of the IPM mentioned at the beginning of this section. When, in addition, the antisymmetry of the many-electron wave function is neglected, all quantities of interest can be obtained by statistical combinations of single-particle probabilities such as the  $p_i^{\text{loss}}$  of Eq. (4). One option is to use standard multinomial statistics [22], which, however, may give substantial contributions for unphysical multiple capture processes that correspond to the formation of negatively charged ions. To overcome this problem we have introduced the analysis in terms of products of binomials in Ref. [6]. This model is used in the present work. Here it is assumed that the formation of negative ions cannot be described within the IPM. The corresponding capture channels are eliminated, and the net electron-capture probability  $P_{\text{net}}^{\text{cap}}$  is distributed over the physical capture channels (i.e., identified with single capture in the case of proton impact and is subdivided into single and double capture events in the case of  $\text{He}^{2+}$ -ion impact). The probabilities for  $k$ -fold capture are then combined with independent probabilities for  $l$ -fold ionization to obtain probabilities and cross sections for charge-state correlated events. The more global  $q$ -fold loss cross sections considered in this paper are obtained by adding the contributing individual cross sections  $\sigma_{kl}$ ,

$$\sigma_q = \sum_{k+l=q} \sigma_{kl}. \quad (6)$$

Since we have found substantial single-particle probabilities for transitions to the unoccupied  $3d$  and  $n=4$  states of Ar at low to intermediate projectile energies, we have also carried out a statistical analysis of multiple-excitation events that might contribute to electron removal via autoionization (AI). In this case we have applied a standard shell-specific binomial analysis for excitation and have added the resulting cross sections for  $m$ -fold excitation  $\sigma_m^{\text{exc}}$  to the net electron loss (+) and ionization (−) cross sections according to

$$\sigma_{\pm}^{\text{AI}} = \sigma_{\pm} + (\sigma_2^{\text{exc}} + \sigma_3^{\text{exc}}) + 2(\sigma_4^{\text{exc}} + \sigma_5^{\text{exc}}) + \dots \quad (7)$$

The multiplicities in Eq. (7) are obtained from the assumption that each pair of excited electrons autoionizes with 100% probability, i.e., the possibility of radiative decay is neglected completely. This is of course an extreme assumption, but probably it is less severe than the IPM itself. In reality, multiply excited bound states are expected to be correlated and to occur with less probability than predicted by independent-particle statistics. For these reasons, the AI model can only be considered to lead to an upper estimate for the contribution of autoionizing states to the net electron removal cross sections.

### III. RESULTS AND DISCUSSION

#### A. $p$ -Ar data

In Fig. 1 results are presented for net electron loss due to capture and ionization in  $p$ -Ar collisions together with the experimental data of Ref. [23]. It can be seen that dynamical

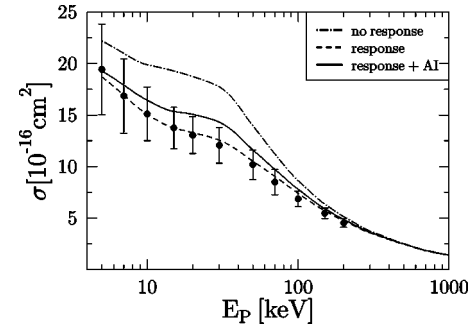


FIG. 1. Total cross section for net electron loss as a function of impact energy for  $p$ -Ar collisions. Theory: present calculations with frozen target potential (no response), with inclusion of the time-dependent target screening model (response), and with additional inclusion of AI processes (response + AI). Experiment: closed circles [23].

electron screening effects at the target are appreciable at energies below 100 keV impact energy, and that they account for a decrease in the cross section by about 20% at energies below 50 keV. It is interesting that the IPM calculation with target screening follows the experiment almost perfectly before an AI correction is applied.

Also included is the dynamical target screening model result with the correction due to multiple  $M$ - and  $N$ -shell excitation described in Sec. II. The AI correction estimate results in an up to 10% increase in the cross section at 10–50 keV impact energy. The correction pushes our data towards the upper bracket of the standard deviation of the experimental data. We suspect that the correction is exaggerated for the reasons given above (while our single-excitation probabilities are probably accurate, it can be expected that binomially calculated multiple excitations are too large). Another possibility might be that the target response model is too weak, and that target polarization effects might lead to a reduced net electron loss cross section before the correction is applied.

In principle, another electron removal effect should be included, namely, Auger decays and shake off in the  $M$  shell following  $L$ -shell vacancy production. However, the  $L$ -shell ionization cross sections are calculated to be small, and therefore this effect is considered to be minor for the net ionization and electron-loss cross sections. The situation is different when one considers  $q$ -fold electron loss with  $q \geq 3$  at higher energies, which is described further below.

In Fig. 2 we show the net ionization cross section for the same three models (no response, target response, target response + AI) for 5–5000 keV impact energy in comparison with experiment [24]. The experimental data display a maximum at 50–70 keV impact energy. The frozen atomic target potential calculation (no response) overestimates the data given here by almost 50%, and peaks at a lower energy. The calculation with spherically symmetric target response reaches the upper limit of the standard deviation of the experimental data in this range, and falls below the experimental data at collision energies below 15 keV. For impact energies above 300 keV, the calculations with and without

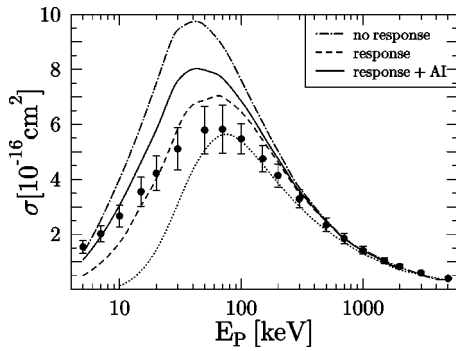


FIG. 2. Total cross section for net ionization as a function of impact energy for  $p$ -Ar collisions. Theory: present calculations with frozen target potential (no response), with inclusion of the time-dependent target screening model (response), and with additional inclusion of AI processes (response + AI); dotted line: CDW-EIS calculation [1]. Experiment: closed circles [24].

response merge and describe the experimental data very well.

The AI contributions are estimated to be significant for collision energies below 100 keV. Upon inclusion of these AI effects, the experimental cross section is overestimated in the 15–100 keV energy range, but they do help in order to explain the ionization data at energies below 15 keV. More experimental data towards lower energies would be of interest in order to investigate the discrepancy in slope between the theoretical and experimental results.

One conclusion that can be drawn at this stage is that one would like to seek clarification of the following issues from future experimental and theoretical works: (1) experiments with improved statistics and range expanded to lower energy; (2) more elaborate response calculations to study the effect of polarization on the suppression of net ionization; (3) an independent confirmation that AI contributes at the 15% level towards net ionization near the maximum, and substantially more at low energies. Nevertheless, we can state that excellent agreement with experiment on the net ionization cross section exists at energies above 100 keV, and that a semiquantitative explanation of the data has been provided for lower energies.

Included in Fig. 2 is a comparison with the continuum-distorted-wave with eikonal initial-state (CDW-EIS) calculation of Ref. [1] performed with orbitals based on the OPM. Several observations can be made when comparing the different calculations. One might think that at high energies the present nonperturbative calculations should agree with this model. It turns out, however, that between 300 keV and 1 MeV impact energy where the effects of target response become very small, the CDW-EIS results are found to lie systematically below the IPM-BGM data. In the vicinity of the maximum of the experimental data, the CDW-EIS results show a dramatic deviation towards lower energies, signaling a failure of this perturbative method. The discrepancy between the theories in the vicinity of the maximum is particularly remarkable, since the perturbative method should be tracking a TDSE calculation without target response.

In Fig. 3 the two relevant model calculations are com-

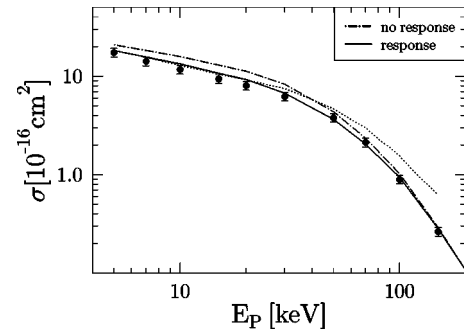


FIG. 3. Total cross section for net electron capture as a function of impact energy for  $p$ -Ar collisions. Theory: present calculations with frozen target potential (no response), and with inclusion of the time-dependent target screening model (response); dotted line: two-center atomic-orbital calculation [26]. Experiment: closed circles [23].

pared with the experimental data of Ref. [23] for net electron capture for 5–150 keV impact energy. Earlier measurements of these cross sections were reviewed in Ref. [25], and are not included in Fig. 3 for the sake of clarity. The majority of them are in agreement with the data of Ref. [23]. The calculation with target response is in good agreement with experiment, although on the high side for impact energies between 8 and 20 keV. The calculation without response is markedly different below 50 keV impact energy. The discrepancy between the two models amounts to about 15% for energies lower than 20 keV.

A recent model potential calculation of capture processes in the  $p$ -Ar system is also available for comparison [26]. An independent-particle model has been set up in this work based on a three-parameter potential adjusted to yield approximately six of the argon energy levels derived from spectroscopy (from  $3s$  up to  $4d$ ). The TDSE has been solved in a two-center atomic-orbital expansion with basis states to represent the  $M$  shell and partially the  $N$  shell in argon, as well as the  $n = 1 - 4$  orbitals of hydrogen. Therefore, in comparison to the present work, this calculation neglects couplings to the continuum, target-response effects, and contributions from the argon  $K$  and  $L$  shells. It can be seen that the model overestimates the experimental data of Ref. [23] by about a factor of 2 for impact energies above 50 keV. This is clearly caused by the neglect of continuum couplings in this calculation, since both of our calculations agree with those experiments in that regime.

Interestingly enough, at 20 keV impact energy and below the model calculation of Ref. [26] is closer to our results with target response. At these energies continuum couplings are believed to be unimportant, so the question arises why the two-center atomic-orbital calculation does not follow our calculation without target response. We have compared the model potential from Ref. [26] with our optimized effective potential which incorporates exchange effects exactly, and have found substantial differences in how that model potential approaches the asymptotic  $-1/r$  limit as compared to our effective potential. The quality of matching experimental spectroscopic data on the occupied and unoccupied Ar levels in the  $M$  and  $N$  shells is comparable, although the individual

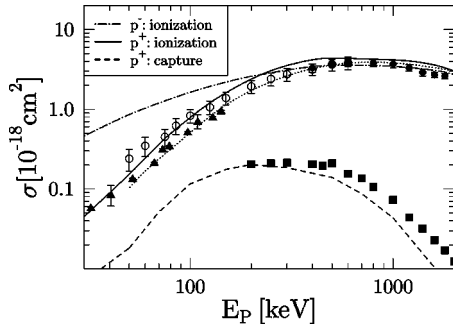


FIG. 4. Total cross sections for net ionization and capture from the Ar( $L$ ) shell as functions of impact energy. Theory: present calculations with inclusion of the time-dependent target screening model for capture and ionization by proton  $p^+$ , and for ionization by antiproton  $p^-$  impact; dotted line: CDW-EIS calculation for net ionization by protons [30]. Experiment: single ionization for proton impact: open circles [27], closed triangles [28], closed circles [29]; single capture for proton impact: closed squares [31].

energy levels are different [the OPM does not match the Ar( $3p$ ) orbital energy very accurately, but overbinds this orbital at the 7% level, namely,  $\epsilon_{3p}^{\text{OPM}} = -0.6205$  vs  $-0.577$  hartree].

Other reasons for why the two calculations cannot be compared directly can be found in the method of solution of the TDSE. The BGM calculation has been shown to reproduce adiabatic molecular orbitals, and it is not obvious that a finite atomic-orbital expansion can achieve this with comparable accuracy. Therefore, the atomic-orbital calculation with a model in which the Ar( $3p$ ) orbital is closer to resonance with H( $1s$ ) than our calculation may have a suppressed charge-transfer cross section as a result of basis limitations when solving the TDSE. We do not present here state-selective capture cross sections, but will report them separately. We note, however, that our H( $n=2$ )-shell capture cross sections are in reasonable agreement with experiment down to the lowest energies shown. In contrast, the data of Ref. [26] overestimate this channel substantially, and have a much lower H( $1s$ ) capture cross section. This fact supports the idea that the two solution methods for the TDSE are rather different.

In Fig. 4 the  $L$ -shell net ionization data are displayed in comparison with experiments for single ionization [27–29]. This comparison is justified, as multiple  $L$ -shell vacancy production by proton impact has a very small probability. It should be noted that no substantial reduction in this cross section is obtained from target response (we have not included the no-response results, as they are very close). This means that on the collision time scale the  $L$  shell experiences only small changes as a result of the  $M$ -shell ionization phenomena. The agreement with experiment is good with an overestimation of the experimental data by 10–15% at the maximum. The cross section is two orders of magnitude smaller than the overall net ionization cross section, and thus,  $L$ -shell vacancy production does not lead to significant Auger decay contributions at intermediate or low energies. The situation is different at higher energies where the  $M$ -shell cross sections fall off more rapidly and Auger pro-

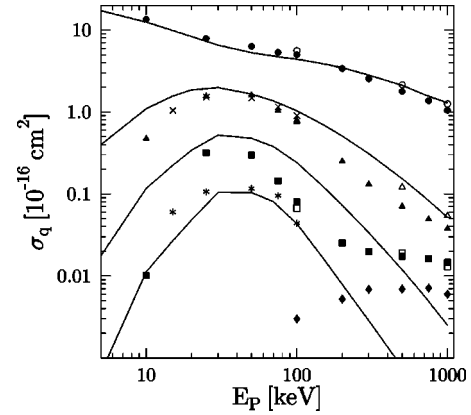


FIG. 5. Total cross sections for  $q$ -fold electron loss  $\sigma_q$  ( $q = 1, \dots, 4$ ) as functions of impact energy for  $p$ -Ar collisions. Theory: present calculations with inclusion of the time-dependent target screening model and with products-of-binomials analysis. The theoretical data correspond to  $q = 1, \dots, 4$  from top to bottom. Experiment: closed symbols [33] with reported errors of  $\pm 15\%$  for  $q = 1, 2$  and up to  $\pm 50\%$  for the higher charge states; open symbols [10] normalized to the theoretical net electron-loss cross section. The error bars are smaller than the size of the symbols. Circles:  $q = 1$ , triangles:  $q = 2$ , squares:  $q = 3$ , diamonds:  $q = 4$ ; crosses and asterisks are extracted from Ref. [32] for  $q = 2$  and  $q = 3$ , respectively, as described in the text.

cesses dominate over direct multiple  $M$ -shell ionization.

The figure includes a comparison with the CDW-EIS calculation of Ref. [30]. The agreement is very good, except at the lowest energies where the distorted wave results drop off more quickly, but much less so than in the case of the  $M$  shell. Also displayed in Fig. 4 is the total cross section for capture from the  $L$  shell. It can be seen that it is responsible for less than 10% of  $L$ -vacancy production over the energy range shown, and that the maximum is rather broad. The IPM-BGM calculations are in good agreement with the experimental data [31] except at the higher energies, where it is possible that the BGM basis states have a difficulty in representing the translational phase for the bound projectile states with sufficient accuracy. The displayed data for  $L$ -shell ionization by antiproton impact are discussed in Sec. III B.

Cross sections for the production of  $q$ -fold charged recoils are provided in Fig. 5. An extensive discussion of various pathways that lead to multiply charged Ar ions can be found in Ref. [32]. Since we are interested in the many-electron aspects of the IPM itself, we do not engage in a detailed discussion of the postcollision effects due to Auger decays and shake off following  $L$ -vacancy production. We also omit the discussion of AI transitions following multiple  $M$ -shell excitation, given that the discussion of the net ionization cross sections indicates that our statistical IPM evaluation appears to result in an overestimation of AI events. However, we note that the effects of AI processes on the  $q$ -fold loss cross sections are likely to be moderate. At low to intermediate impact energies where we have found substantial AI contributions to net ionization, the capture channel dominates the  $q$ -fold loss. In fact, a few test calculations confirmed the minor importance of AI processes.

The following observations can be made when comparing our data with experiment. The  $q=1$  channel is described very well. For the  $q=2$  channel we have a systematic discrepancy with the experiment of Ref. [33] at impact energies above 100 keV. In order to understand this discrepancy, we have included two other experimental datasets: the data for single capture accompanied by single ionization, double capture and direct double ionization given in Fig. 5 of Ref. [32] have been added to provide independent data in the 15–100 keV energy range. Also the data of Ref. [10] for cross-section ratios  $\sigma_q/\sigma_1$  between 100 and 1000 keV have been normalized to our net cross section and are included in Fig. 5. These additional data lend some credibility to the calculated  $q=2$  cross sections from the present work, but new experimental work is required to provide more clarity on this issue.

In order to obtain good agreement with experiment at energies below 30 keV for the  $q=2$  channel, it is important to use the products-of-binomials analysis introduced in Ref. [6]. The standard trinomial analysis (not shown) overestimates  $q$ -fold loss for  $q \geq 2$  at low energies by predicting a strong double-capture probability into  $H^-$  at small impact parameters. While  $H^-$  formation is a relevant channel [32], it cannot be calculated reliably without taking final-state correlations into account. The products-of-binomials analysis simply eliminates this channel and redistributes the flux. At 10 keV and below, this model still appears to overestimate  $q=2$  recoil ion production by at least a factor of 2.

The  $q=3$  channel displays a serious failure of the IPM. While the experimental  $\sigma_3$  data points of Ref. [33] at 25 and 50 keV impact energy come close to our theoretical results, it should be noted that they are known to be too high, given that the partial contributions to this channel are well known from other experiments, and do not add up to those values [32]. Indeed, when we compare with the sum of the partial cross sections for energies between 20 and 200 keV, we find that the shape of the theoretical cross section is quite realistic, but that the absolute magnitude is higher by a factor of 3.

The  $q=4$  IPM cross section is higher by a much larger factor. These observations indicate that a complete breakdown occurs in the model, and that one should not take the IPM predictions for these channels seriously. The  $q=4$  channel is apparently completely dominated by Auger decays and shake off, namely, vacancy production in the  $L$  shell (resulting in two or more continuum electrons) with simultaneous, predominantly, double ionization of the  $M$  shell.

For energies above 200 keV, the experimental data indicate a strong presence of Auger decays also for the lower recoil charges  $q$ . Following the discussion of Ref. [32], and particularly the previous investigations of Ref. [34] and other works cited there, one can model the decays by a shell-specific binomial analysis: a single  $L$ -vacancy decays by Auger and Coster-Kronig transitions resulting in 71% double vacancy, 27% triple vacancy, and 3% quadruple vacancy. Assuming that one can combine this information with independent  $M$ -vacancy formation during the collision, one can carry out a complete analysis. We have carried out a test calculation at 300 keV, and found that the  $q=1$  channel remained unaffected, the  $q=2$  channel experienced a few-percent de-

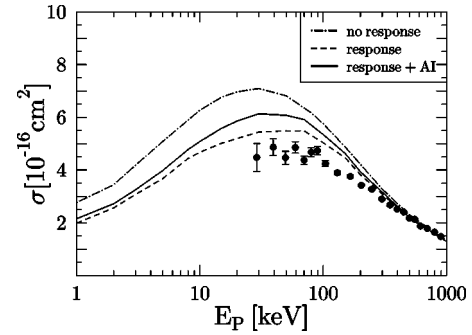


FIG. 6. Total cross section for net ionization as a function of impact energy for  $\bar{p}$ -Ar collisions. Theory: present calculations with frozen target potential (no response), with inclusion of the time-dependent target screening model (response), and with additional inclusion of AI processes (response + AI). Experiment: closed circles are calculated from the data of Ref. [16] according to  $\sigma_{\text{net}} = \sigma_1 + 2\sigma_2 + 3\sigma_3$ .

crease, while the  $q=3$  channel increased by a factor of 2–3. Given that our IPM triple  $M$ -shell vacancy production probabilities are much too large to begin with, it is pointless to carry out this analysis. Nevertheless, the change in the shape of the  $q$ -fold electron-loss cross section at energies above 200 keV can be understood in principle in this way: the  $L$ -vacancy production cross section shown in Fig. 4 becomes significant at these energies, and drops off above 1 MeV.

### B. $\bar{p}$ -Ar data

In this section we show the net ionization and multiple-ionization cross sections for argon targets following antiproton impact. In Fig. 6 the net ionization cross section for the three models (no response, target response, and target response + AI) is compared with the experiment of Ref. [16]. The difference between the no-response and target-response model results is somewhat smaller than for  $p$ -Ar collisions. Above 300 keV impact energy, the three models coalesce and agree very well with experiment. Between 100 and 300 keV, the models predict somewhat higher cross sections than reported by experiment—an effect that is more pronounced than in the  $p$ -Ar case. An almost flat plateau emerges at energies between 15 and 100 keV, which is different from the  $p$ -Ar system in which capture begins to dominate at low energies resulting in a decrease of the ionization cross section, and therefore leading to a pronounced maximum.

As discussed in the context of Fig. 1 for  $p$ -Ar, we can expect the best model result to lie between the middle and bottom curves, as the AI transitions are likely to be overestimated. The data for the  $q$ -fold ionization indicate that the dominant  $q=1$  channel represents the source of the discrepancy at 80–250 keV impact energy. However, this channel should be the one calculated most reliably.

In Fig. 7 the multiple-ionization cross sections are compared for  $q=1,2,3$ . We have included the AI effects by performing a trinomial analysis for  $m$ -fold excitation along with  $l$ -fold direct ionization, and by interpreting the results along the same lines as described in Sec. II for the case of net ionization. The graphs show clearly that the single-ionization

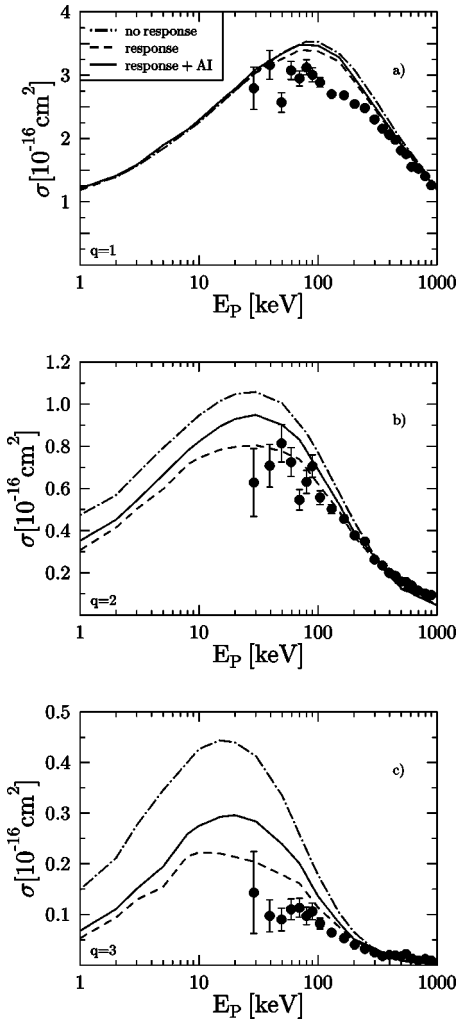


FIG. 7. Total cross sections for (a) onefold, (b) twofold, and (c) threefold ionization as functions of impact energy for  $\bar{p}$ -Ar collisions. Theory: present calculations with frozen target potential (no response), with inclusion of the time-dependent target screening model (response), and with additional inclusion of AI processes (response + AI). The cross sections are evaluated with the shell-specific binomial and trinomial analyses. Experiment: closed circles [16].

channel is least affected by response and AI effects. These nonperturbative phenomena arise at small and intermediate impact parameters when multielectron processes can compete against one-electron transitions. We note that the twofold ionization cross sections display very good agreement with experiment. This fact makes us believe strongly in our single-ionization results, because it would be curious indeed, if an IPM managed to predict double ionization, but not single ionization.

For the triple-ionization channel, we make the observation that the difference between the calculations without and with target response is rather substantial (factor of 2 between 10 and 40 keV). Also, the agreement of the calculation with response before AI corrections with the experiment is quite good for impact energies above 80 keV, which reinforces the argument about the quality of our net ionization and single-

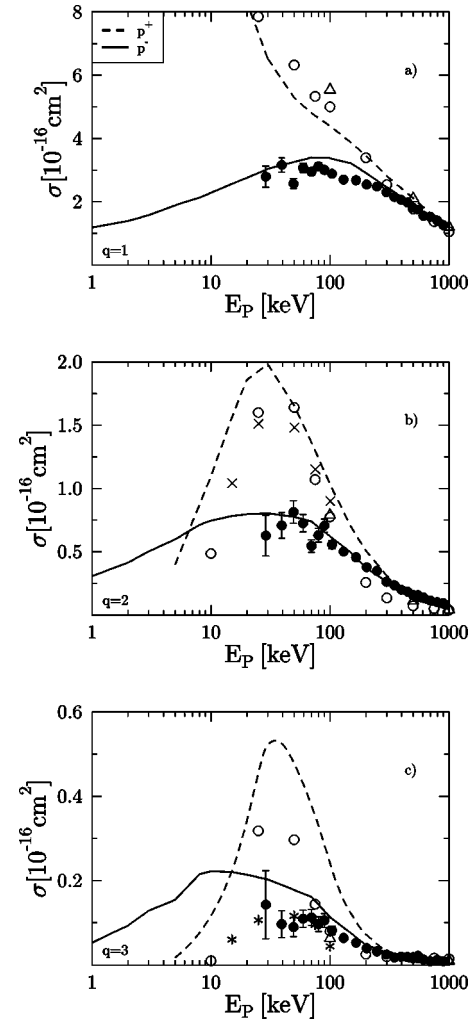


FIG. 8. Total cross sections for (a) onefold, (b) twofold, and (c) threefold electron loss as functions of impact energy for  $p, \bar{p}$ -Ar collisions. Theory: present calculations with inclusion of the time-dependent target screening model and with shell-specific binomial analysis for antiproton ( $p^-$ ) and products-of-binomials analysis for proton ( $p^+$ ) impact. Experiment: antiproton impact: closed circles [16]; proton impact: open circles [33] with reported errors of  $\pm 15\%$  for  $q=1,2$  and up to  $\pm 50\%$  for  $q=3$ ; open triangles [10] normalized to the theoretical net electron-loss cross section. The error bars are smaller than the size of the symbols; crosses and asterisks are extracted from Ref. [32] for  $q=2$  and  $q=3$ , respectively, as described in the text.

ionization result. It is remarkable that while the  $p$ -Ar threefold electron-loss cross section is deemed to be too high by a factor of about 3 at 100 keV impact energy, the present result for  $\bar{p}$ -Ar is rather close to experiment. It appears as if experimentally the results for proton and antiproton impact removal are very comparable in this channel, while our IPM theory predicts that threefold loss due to proton impact (mostly from the  $M$ -shell) is stronger by a factor of 2–3.

In Fig. 8 we display the direct comparison of proton and antiproton impact electron loss for  $q=1,2,3$  on a linear scale. Shown are the calculations with target response (excluding AI corrections). For medium and high energies, the IPM-

BGM results predict that protons are more efficient in removing electrons than antiprotons, with merging results only at the highest impact energy shown, i.e., at 1 MeV. This finding is consistent for all charge states  $q=1,2,3$ .

The experimental data show quite different behavior for the different recoil charge states. They probably do not have sufficient absolute accuracy in order to determine unambiguously at which energies they merge (e.g., are within a few percent of each other). For proton projectiles we have three independent datasets, one of which [33] is in conflict with the other two [10,32] in the case of  $q=2,3$ . For the single-electron-loss channel we find that experiment and theory follow similar trends, but that the observational data separate unambiguously only for energies below 250 keV.

For  $q=2$  the experimental data for proton projectiles of Ref. [33] are a factor of 2 below the antiproton data for energies above 100 keV. When we add the partial cross sections given in Ref. [32] for 15–100 keV impact energy, we find them to be reasonably close to the theory. The data of Ref. [10] for proton impact is below the antiproton impact result, but definitely closer than a factor of 2 in the 100–1000 keV energy range. In Refs. [10,16] arguments were provided for why the  $\sigma_2/\sigma_1$  ratio should be higher for antiprotons than for protons (while the  $\sigma_3/\sigma_1$  ratio would be the same for both projectiles), but we note that the arguments are based on perturbation theory (interference of scattering amplitude contributions), and also on the complete domination of the  $q=3$  channel by inner-shell vacancy production and subsequent decays. Therefore, the arguments apply to the higher end of the energy scale considered in this paper, and are not necessarily relevant at energies up to several hundred keV.

The  $q=3$  data show the proximity of the experimental  $p$ -Ar and  $\bar{p}$ -Ar data around 100 keV, and even below, if one discounts the data of Ref. [33]. The big discrepancy in the theoretical results for the two projectiles is also apparent. Thus, one finds that one selection of experiments supports the notion of nearly identical  $q=2,3$  loss cross sections for  $p$  and  $\bar{p}$  impact at energies above 100 keV, while theory displays a substantially increased efficiency of multiple-electron removal by proton impact, particularly in the  $q=3$  channel. This difference then leads to the apparent conclusion that the antiproton electron-loss data can be explained up to  $q=3$ , while the proton data are explained only up to  $q=2$  at intermediate energies. Even at  $q=2$  the proton data are overestimated somewhat by the IPM theory.

In order to summarize the comparison of theory and experiments at 100 keV impact energy, we note that the ratio  $R_2 = \sigma_2/\sigma_1$  is already overestimated by theory: we calculate  $R_2^{\text{th}} = 0.235$  as compared to  $R_2^{\text{exp}} = 0.15$  given by Refs. [10,33]. For antiprotons we obtain  $R_2^{\text{th}} = 0.18$ , which compares well with  $R_2^{\text{exp}} = 0.19$ . For  $R_3 = \sigma_3/\sigma_1$  we find for proton impact  $R_3^{\text{th}} = 0.055$ , which is far in excess of the experimental values of  $R_3^{\text{exp}} = 0.016$  [33] and  $R_3^{\text{exp}} = 0.012$  [10], respectively. For antiprotons we have  $R_3^{\text{th}} = 0.034$ , which is not too far off from  $R_3^{\text{exp}} = 0.028$  [16].

This observation then leads to the remarkable statement that electron correlations are very strong at the level of three-

electron processes for proton impact, but not for antiproton impact. One possible cause for such a difference in behavior could be the fact that proton impact leads to an attraction of electrons (which forces them to correlate), while antiproton impact pushes the electrons away, thereby diminishing the role of correlations. Not only does this geometric phenomenon result in a smaller cross section for antiproton impact, but it could also explain the reduced importance of deviations from IPM-type behavior in this case. The idea that electronic correlations are less important in atomic collisions with antiparticles than with particles has been proposed before in the context of two-electron helium targets for which correlated calculations can be performed [35,36].

The comparison of the theoretical data at low energies shows that protons are much more efficient at producing a single vacancy in Ar due to single capture, but that the situation reverses as one increases the multiplicity. Antiprotons are found to be more efficient in producing multiple vacancies at low energies due to ionization, which is suppressed in the case of protons due to the strong single-capture channel. Our result for  $q=2,3$  excludes formation of the negative hydrogen ion, which has, however, a rather small cross section [32]. Of course, these findings could be an artifact of the IPM, and therefore the experimental investigation of a careful comparison of these cross sections would be of great interest.

Finally, we comment on the  $L$ -shell ionization cross section induced by antiprotons, which is compared with the relevant proton-impact data in Fig. 4. We observe that antiprotons are more efficient in ionizing an  $L$ -shell electron than protons at impact energies below 200 keV. This feature is also visible in the overall ionization (cf. Figs. 2 and 6), but is masked when one considers electron loss (Fig. 8) due to the strong single-capture channel in the case of proton impact.  $L$ -shell capture, however, is very weak due to the large energy defect between the tightly bound target electrons and the available projectile states, and, as a consequence, antiprotons are more efficient in producing  $L$ -shell vacancies than protons. This is a clean manifestation of what has been called the binding/antibinding effect [37]: At low impact energies, the cross section is dominated by close collisions with impact parameters smaller than or comparable to the mean radius of the target orbitals. In such collisions, antiprotons weaken the binding of the electrons and make ionization more likely than impinging protons.

Around 200 keV, the proton- and antiproton-impact data cross and appear to merge only at energies higher than the ones considered in the figure; i.e., the Born limit is approached at higher impact energies than in the case of the overall ionization (cf. Fig. 8). This is of course no surprise, given that the average velocity of the  $L$ -shell electrons is much higher than that of the  $M$  shell.

### C. He<sup>2+</sup>-Ar data

In Fig. 9 we show the electron-loss cross sections due to capture and ionization in 5–1000 keV/amu He<sup>2+</sup>-Ar collisions. The findings are similar to the  $p$ -Ar case displayed in Fig. 9. The no-response calculation overestimates experiment

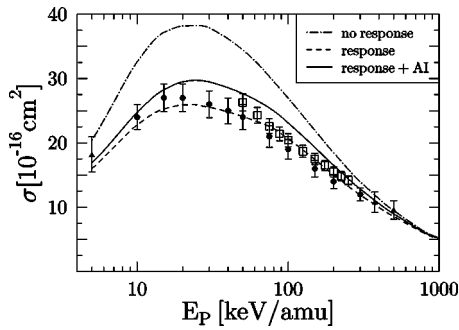


FIG. 9. Total cross section for net electron loss as a function of impact energy for  $\text{He}^{2+}$ -Ar collisions. Theory: present calculations with frozen target potential (no response), with inclusion of the time-dependent target screening model (response), and with additional inclusion of AI processes (response + AI). Experiment: closed circles [8], closed triangles [9], and open squares [38].

at the broadened maximum (10–50 keV/amu impact energy) by 30% in this case. The calculation with target response is in good agreement with the experimental data over the entire energy range. The AI correction estimate increases the results by about 15% for 10–100 keV/amu impact energies and leads to marginal agreement with experiment.

The comparison with the  $p$ -Ar data in Fig. 1 reveals that the cross section begins to drop for energies smaller than 15 keV/amu. This trend (which is the result of nonresonant capture that peaks rather than rising at low energies) is described very consistently by the response model when compared with experiment. This leads to the remarkable result that at 5 keV/amu impact energy, i.e., for comparable velocities, proton and  $\text{He}^{2+}$  projectiles are equally efficient in removing electrons from argon targets.

In Fig. 10 we compare the net ionization cross sections. The experimental datasets have almost overlapping statistical error bars for most energies with some wider discrepancies at the lower end of the energy range displayed. The calculation with target response is in good agreement with them at intermediate to high energies, and falls short at the lowest energies. The AI contributions are estimated to be about 15% for energies between 40 and 100 keV/amu, and substantially

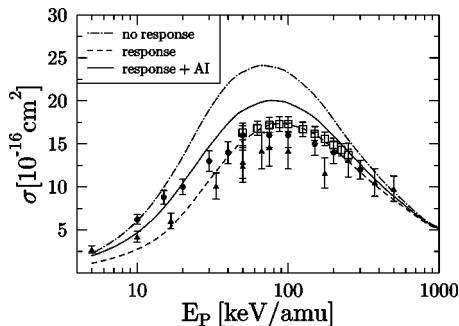


FIG. 10. Total cross section for net ionization as a function of impact energy for  $\text{He}^{2+}$ -Ar collisions. Theory: present calculations with frozen target potential (no response), with inclusion of the time-dependent target screening model (response), and with additional inclusion of AI processes (response + AI). Experiment: closed circles [8], closed triangles [9], and open squares [38].

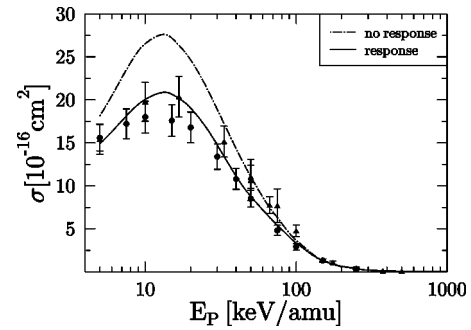


FIG. 11. Total cross section for net electron capture as a function of impact energy for  $\text{He}^{2+}$ -Ar collisions. Theory: present calculations with frozen target potential (no response) and with inclusion of the time-dependent target screening model (response). Experiment: closed circles [8], closed triangles [9].

more at lower energies in accord with the  $p$ -Ar results. At the maximum (40–100 keV/amu) they lead to a significant overestimation of the cross section at the level of 2–3 standard deviations when compared to the experimental data of Ref. [38]. Therefore, one has to question the validity of the statistical IPM estimation of multiple excitations based on single-particle excitation probabilities. One can assume that the correct theoretical data lie between the lowest two curves displayed.

A comparison of the theoretical net ionization data for the  $p$ -Ar and  $\text{He}^{2+}$ -Ar systems before the AI correction is applied reveals that in both cases, target response provides a shift of the maximum of the cross section: from about 45 keV towards 65 keV in the case of  $p$ -Ar, and from 65 keV/amu towards 85 keV/amu in the  $\text{He}^{2+}$ -Ar case. In both cases the shift is required in order to obtain agreement with experiment. The ratio of the cross sections of the doubly to singly charged projectile case at the respective maximum is about 2.4 for both IPM-BGM calculations with and without target response. The experimental data are fully consistent with this ratio (given their relative discrepancies and statistical error bars). It is remarkable that the inclusion of target response results in a reduction of the cross section at maximum by about 30% for both projectiles, such that the cross-section ratio remains the same.

In Fig. 11 the net capture data are shown. The difference between the no-response and target-response calculations is significant for energies below 100 keV/amu. For energies less than 20 keV/amu, the discrepancy has grown to at least 30%, and the agreement of the better calculation with experiment is gratifying. At the lower energies the collision is sufficiently slow such that the change in the atomic structure due to the dynamical ionization process after the closest approach has a chance to modify the electron transfer process. Note how the net capture cross section continues to rise in the  $p$ -Ar calculation (with and without response), while it turns around in the present case for energies below 10 keV/amu.

In Fig. 12 our  $q$ -fold electron-loss data for the model with target response without AI corrections and with product-of-binomials evaluation is compared to the experimental data of

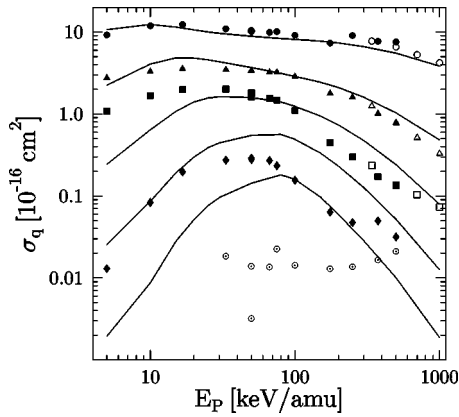


FIG. 12. Total cross sections for  $q$ -fold electron loss  $\sigma_q$  ( $q = 1, \dots, 5$ ) as functions of impact energy for  $\text{He}^{2+}$ -Ar collisions. Theory: present calculations with inclusion of the time-dependent target screening model and with products-of-binomials analysis. The theoretical data correspond to  $q = 1, \dots, 5$  from top to bottom. Experiment: closed symbols and ( $\odot$ ) [9] with reported errors of  $\pm 15\%$  for  $q = 1, 2, 3$  and up to  $\pm 30\%$  for the higher charge states; open symbols [10] normalized to the theoretical net electron-loss cross section. The error bars are smaller than the size of the symbols. Circles:  $q = 1$ , triangles:  $q = 2$ , squares:  $q = 3$ , diamonds:  $q = 4$ , and open circles with dots:  $q = 5$ .

Ref. [9], and to the relative data of Ref. [10], which were normalized to our net cross section. We note that in contrast to the  $p$ -Ar data, the experimental cross sections show much less evidence for the importance of Auger decays and shake-off processes at high energies. This is due to a much stronger presence of direct multiple ionization from the  $\text{Ar}(M)$  shell.

The calculated  $q = 1$  channel shows reasonable agreement with the data that are deemed to be accurate at the 10–15 % level. When compared to experiment, the theoretical data are on the low side for intermediate to high energies, which leaves some room for AI contributions following double excitation in the  $\text{Ar}(M)$  shell.

For the  $q = 2$  channel we find acceptable agreement, except that the shape of the cross section is somewhat different. The theoretical data display a broad maximum at energies of 10–30 keV/amu, while the data of Ref. [9] are remarkably constant for 10–100 keV/amu. At energies above 200 keV/amu, the theoretical data overestimate both experimental datasets with a discrepancy that grows with energy, i.e., the measured data fall off more rapidly with energy.

A marked discrepancy is noted between theory and experiment for the  $q = 3$  channel, i.e., three-electron removal from Ar. While the results are in good accord for 50–100 keV impact energies, the theoretical data underestimate this channel badly at low energies and overestimate it by up to a factor of two for  $E \geq 200$  keV/amu. The two data points at 700 and 1000 keV/amu, respectively, may, in fact, signal the onset of appreciable Auger decay contributions.

The discrepancy at low energies was to be expected, following the analysis of the more detailed experimental data available in Ref. [9]. It has been noted in the experimental data at 5–10 keV energy that direct ionization is practically nonexistent there, while single capture is accompanied by an

additional ionization event in one out of six times, and double capture is accompanied by an additional ionization event in typically 40% of the cases. This behavior cannot follow directly from an IPM in which a pair of single-particle probabilities for ionization and capture relates the three channels. We note that for the  $\text{He}^{2+}$ -Ne collision system [7], the  $q = 3$  cross section behaves very differently at low energies: both the experimental and theoretical data decrease substantially with decreasing energy, and are in agreement.

It is evident that in the  $\text{He}^{2+}$ -Ar case the strong increase in the  $q = 3$  channel goes together with a depression in the experimental  $q = 2$  cross section, i.e., there is ample evidence that the  $q = 3$  channel has grown at the expense of the  $q = 2$  channel at low energies. One explanation for the distinct behavior of the double-capture channel at low energies is in terms of adiabatic curve crossings provided along with experimental data in Ref. [39]. Here it was argued that AI events should not be the reason for the strong amount of  $M$ -shell ionization that accompanies double capture due to the small probability for simultaneous double excitation together with two-electron capture. The adiabatic electron energy curves as a function of internuclear separation included the possibility for single ionization following double capture to the  $\text{He}(1s^2)$  ground state. Another mechanism for electron emission is a shake process following capture from the  $3s$  level of Ar. Vacancy production in this subshell has been assigned a 13.5% conversion probability in photoionization experiments [40].

To shed some light on the situation within the IPM, we looked for clues in the separate single-electron capture probabilities from the  $3s$  and  $3p$  levels of Ar. We found that the double-capture channel has a substantial contribution from simultaneous capture from both levels. At 50 keV/amu impact energy, the contributions are found to be equal, with a gradual decline of capture from  $(3s3p)$  with decreasing energy. At 5 keV/amu the double capture channel is predicted to originate three out of four times from the  $(3p^2)$  subshell configuration.

The energy curves given in Ref. [39] suggest that about 5 eV energy has to be provided from the internuclear motion in order to populate the  $\text{He}(1s^2) + \text{Ar}^{3+}$  channel. Given the sequence of ionization energies of 15.8, 27.6, and 40.7 eV for Ar,  $\text{Ar}^+$ , and  $\text{Ar}^{2+}$ , respectively [41], this means that double capture to the  $\text{He}(1s^2) + \text{Ar}^{2+}$  configuration requires a disposal of about 35 eV energy. Thus, it can be argued that in the quasiadiabatic regime, the former channel will be favored due to the energetic proximity in the energy curve diagram. The population of the  $\text{He}(1s^2) + \text{Ar}^{2+}$  channel will be favored when the double capture is from the  $(3s3p)$  subshells, because about 15 eV less electronic energy is available in this case. For the  $\text{He}(1s^2) + \text{Ne}^{2+/3+}$  configuration, the situation is entirely different, because neon atoms are much harder to ionize (the sequence of ionization energies is given as 21.6, 41.0, and 63.5 eV respectively for Ne,  $\text{Ne}^+$ , and  $\text{Ne}^{2+}$  [41]). Therefore, we can use the IPM analysis to at least point the finger at the mechanism of quasiadiabatic correlations as a possible cause for the very different behavior of double capture at low energies with neon and argon

atoms. It would be of interest to carry out detailed many-electron calculations in a quasimolecular basis in order to test this conjecture.

One of our expectations following the work with Ne targets [7,11] has been that a higher projectile charge should make more multielectron transition channels amenable to an IPM description. The present  $q=4$  data support this conclusion to the extent that at low to intermediate energies, qualitative agreement within a factor of 2 can be found. For energies above 100 keV/amu, the IPM prediction for direct multiple ionization is much too high, while the experimental data show evidence for Auger transitions following  $L$ -shell vacancy production. The  $q=5$  data for the  $\text{He}^{2+}$ -Ar system show complete disagreement, as was found for the  $q=4$  channel for proton impact.

#### IV. CONCLUSIONS

We have demonstrated in the present work that the IPM-BGM calculations for bombardment of small atoms (neon and oxygen) by light ions were successfully extended to the case of argon targets. In particular, we have studied the effects of target response, namely, the change of the effective potential with the degree of ionization during the collision in a mean-field model. It was found that this dynamical screening effect is important in order to obtain the correct position and height for the maxima in the net ionization cross sections, and for the correct net capture cross sections as well. For inner-shell processes [the  $\text{Ar}(L)$  shell in particular], the response was found to be irrelevant.

While the global cross sections have been obtained satisfactorily, some unresolved issues remain in the area of the effect of autoionizing and Auger transitions following multiple ionization, and  $L$ -shell vacancy production, respectively. In particular, for the  $p$ -Ar case the  $q$ -fold loss cross sections for  $q \geq 3$  begin to be dominated by Auger decays at energies above 200 keV/amu. In the case of  $\text{He}^{2+}$  impact this occurs for  $q \geq 4$ . Therefore, the IPM calculation needs to be supplemented by an Auger decay model.

It is found that the direct multiple  $M$ -shell effects are overestimated by the IPM beginning with multiplicities of  $n \geq 3$ . This is a signature of strong electron correlation effects that apparently cannot be described by a statistical IPM including dynamical screening. The correlation effects are less important when the target atom is perturbed more strongly, but on the other hand, some marked disagreements were observed in the  $q=3$  channel following collisions with  $\text{He}^{2+}$  particles both at low and at high energies. At low energies, the experimental data are likely to show evidence for quasiadiabatic correlations.

Throughout this paper we have taken the attitude that significant deviations from the present IPM results provide an indication that electron correlations become crucial in the affected channels. Two main issues are important in this respect. On one hand, there is the question whether we have calculated the best-possible time-dependent density  $n(\mathbf{r}, t)$ . On the other hand, there remains the problem of how to extract the information from the single-particle calculations.

As mentioned above, all information should be available from the exact density, but prescriptions for the extraction of this information are only available for rather global quantities, such as the net cross sections.

Our agreement on the net cross sections is good. This suggests that we have obtained a reasonable density from our IPM calculation. One should keep in mind, however, that the channels deemed to be affected by correlations have a small influence on the net cross sections, and therefore, a very careful comparison beyond the available experimental accuracy would be required in order to make this point with certainty. Concerning the more detailed comparisons, such as for  $q$ -fold electron loss, we are using simple evaluations (such as the products-of-binomials analysis) that require a physical interpretation of the single-electron orbitals of the IPM. It is the inaccuracy of these evaluation procedures that is most likely to be responsible for the failure to provide the correct answers.

From the comparison of our works with neon and argon target atoms, we can conclude that the issue of the importance of electronic correlations does not depend strongly on the number of available target electrons. The calculations for neon as well as argon targets display a breakdown of similar magnitude for processes with multiplicities of order  $q \geq 3$ . This result is somewhat unexpected, as one might have argued that the statistical IPM description is more appropriate in the case of argon.

Some future theoretical and experimental work is needed to elucidate the role of vacancy production following multiple excitation in the  $\text{Ar}(M)$  shell. It appears as if the present approach within the statistical IPM overestimates the significance of these phenomena, which causes uncertainty in the theoretical cross sections in the 10–100 keV/amu range. With regard to the  $\bar{p}$ -Ar data we hope that the new experiments planned by the ASACUSA collaboration will shed light on the question whether single (and net) ionization between 100 and 200 keV impact energy will remain a source of discrepancy between theory and experiment. At impact energies below 10 keV, an interesting subject to study is the question of efficiency of multiple vacancy production by  $p$  and  $\bar{p}$  impact given that electron correlations should offer some surprises in this area.

Further measurements of multiple ionization by antiproton impact at intermediate energies should also shed light on the question for which multiplicity electronic correlations become important. In contrast with the case of proton impact we have found that the  $q=3$  channel is well described by the IPM. It would be of interest to determine whether fourfold ionization as a direct multiple-ionization process has a measurable cross section that could be compared to the IPM-BGM results.

#### ACKNOWLEDGMENTS

This work was supported by the Leibniz-Programm of the Deutsche Forschungsgemeinschaft and the Natural Sciences and Engineering Research Council of Canada.

- [1] T. Kirchner, L. Gulyás, H. J. Lüdde, A. Henne, E. Engel, and R. M. Dreizler, *Phys. Rev. Lett.* **79**, 1658 (1997).
- [2] T. Kirchner, L. Gulyás, H. J. Lüdde, E. Engel, and R. M. Dreizler, *Phys. Rev. A* **58**, 2063 (1998).
- [3] T. Kirchner, H. J. Lüdde, and R. M. Dreizler, *Phys. Rev. A* **61**, 012705 (2000).
- [4] H. J. Lüdde, A. Henne, T. Kirchner, and R. M. Dreizler, *J. Phys. B* **29**, 4423 (1996).
- [5] O. J. Kroneisen, H. J. Lüdde, T. Kirchner, and R. M. Dreizler, *J. Phys. A* **32**, 2141 (1999).
- [6] T. Kirchner, H. J. Lüdde, M. Horbatsch, and R. M. Dreizler, *Phys. Rev. A* **61**, 052710 (2000).
- [7] T. Kirchner, M. Horbatsch, H. J. Lüdde, and R. M. Dreizler, *Phys. Rev. A* **62**, 042704 (2000).
- [8] M. E. Rudd, T. V. Goffe, and A. Itoh, *Phys. Rev. A* **32**, 2128 (1985).
- [9] R. D. DuBois, *Phys. Rev. A* **36**, 2585 (1987).
- [10] L. H. Andersen, P. Hvelplund, H. Knudsen, S. P. Møller, A. H. Sørensen, K. Elsener, K.-G. Rensfelt, and E. Uggerhøj, *Phys. Rev. A* **36**, 3612 (1987).
- [11] T. Kirchner, M. Horbatsch, and H. J. Lüdde, *Phys. Rev. A* **64**, 012711 (2001).
- [12] T. Kirchner and M. Horbatsch, *Phys. Rev. A* **63**, 062718 (2001).
- [13] M. E. Rudd, T. V. Goffe, A. Itoh, and R. D. DuBois, *Phys. Rev. A* **32**, 829 (1985).
- [14] R. D. DuBois, *Phys. Rev. A* **39**, 4440 (1989).
- [15] A. C. F. Santos, W. S. Melo, M. M. Sant'Anna, G. M. Sigaud, and E. C. Montenegro, *Phys. Rev. A* **63**, 062717 (2001).
- [16] K. Paludan, H. Bluhme, H. Knudsen, U. Mikkelsen, S. P. Møller, E. Uggerhøj, and E. Morenzoni, *J. Phys. B* **30**, 3951 (1997).
- [17] E. Runge and E. K. U. Gross, *Phys. Rev. Lett.* **52**, 997 (1984).
- [18] J. D. Talman and W. F. Shadwick, *Phys. Rev. A* **14**, 36 (1976).
- [19] E. Engel and S. H. Vosko, *Phys. Rev. A* **47**, 2800 (1993).
- [20] E. Engel and R. M. Dreizler, *J. Comput. Chem.* **20**, 31 (1999).
- [21] E. K. U. Gross, J. F. Dobson, and M. Petersilka, in *Topics in Current Chemistry*, edited by R. F. Nalewajski (Springer, Heidelberg, 1996), Vol. 181, p. 81.
- [22] M. Horbatsch, *Phys. Lett. A* **187**, 185 (1994).
- [23] M. E. Rudd, R. D. DuBois, L. H. Toburen, C. A. Ratcliffe, and T. V. Goffe, *Phys. Rev. A* **28**, 3244 (1983).
- [24] M. E. Rudd, Y.-K. Kim, D. H. Madison, and J. W. Gallagher, *Rev. Mod. Phys.* **57**, 965 (1985).
- [25] H. Tawara and A. Russek, *Rev. Mod. Phys.* **45**, 178 (1973).
- [26] A. Amaya-Tapia, H. Martínez, R. Hernández-Lamonedá, and C. D. Lin, *Phys. Rev. A* **62**, 052718 (2000).
- [27] N. Stolterfoht, D. Schneider, and P. Ziem, *Phys. Rev. A* **10**, 81 (1974).
- [28] M. E. Rudd, *Phys. Rev. A* **10**, 518 (1974).
- [29] W. M. Ariyasinghe, H. T. Awuku, and D. Powers, *Phys. Rev. A* **42**, 3819 (1990).
- [30] L. Gulyás, P. D. Fainstein, and A. Salin, *J. Phys. B* **28**, 245 (1995).
- [31] M. Rødbro, E. H. Pedersen, C. L. Cocke, and J. R. Macdonald, *Phys. Rev. A* **19**, 1936 (1979).
- [32] R. D. DuBois and S. T. Manson, *Phys. Rev. A* **35**, 2007 (1987).
- [33] R. D. DuBois, L. H. Toburen, and M. E. Rudd, *Phys. Rev. A* **29**, 70 (1984).
- [34] R. Hippler, J. Bossler, and H. Lutz, *J. Phys. B* **17**, 2453 (1984).
- [35] T. Bronk, J. F. Reading, and A. L. Ford, *J. Phys. B* **31**, 2477 (1998).
- [36] C. Díaz, F. Martín, and A. Salin, *J. Phys. B* **35**, 2555 (2002).
- [37] P. Hvelplund *et al.*, *J. Phys. B* **27**, 925 (1994).
- [38] L. J. Puckett, G. O. Taylor, and D. W. Martin, *Phys. Rev.* **178**, 271 (1969).
- [39] P. Moretto-Capelle, D. Bordenave-Montesquieu, A. Bordenave-Montesquieu, and M. Benhenni, *J. Phys. B* **31**, L423 (1998).
- [40] T. A. Carlson, W. E. Hunt, and M. O. Krause, *Phys. Rev.* **151**, 41 (1966).
- [41] A. A. Radzig and B. M. Smirnov, *Reference Data on Atoms, Molecules, and Ions*, Springer Series in Chemical Physics Vol. 31 (Springer, Berlin, 1985).